Dimensionality of Rolled-up Nanomembranes Controls Neural Stem Cell Migration Mechanism

Britta Koch,*,[†] Anne K. Meyer,[†,‡] Linda Helbig,[†] Stefan M. Harazim,[†] Alexander Storch,[‡,§,⊥] Samuel Sanchez,[†,¶] and Oliver G. Schmidt[†,‖,#]

[†]Institute for Integrative Nanosciences, Leibniz Institute for Solid State and Materials Research Dresden, D-01069 Dresden, Germany

[‡]Division of Neurodegenerative Diseases, Department of Neurology, Technische Universität Dresden, D-01307 Dresden, Germany

[§]German Center for Neurodegenerative Diseases (DZNE) Dresden, D-01307 Dresden, Germany

[⊥]Center for Regenerative Therapies Dresden (CRTD), Technische Universität Dresden, D-01307 Dresden, Germany

[¶]Max Planck Institute for Intelligent Systems, D-70569 Stuttgart, Germany

[‖]Material Systems for Nanoelectronics, Technische Universität Chemnitz, D-09107 Chemnitz, Germany

[#]Center for Advancing Electronics Dresden, Technische Universität Dresden, D-01187 Dresden, Germany

S Supporting Information

ABSTRACT: We employ glass microtube structures fabricated by rolled-up nanotechnology to infer the influence of scaffold dimensionality and cell confinement on neural stem cell (NSC) migration. Thereby, we observe a pronounced morphology change that marks a reversible mesenchymal to amoeboid migration mode transition. Space restrictions preset by the diameter of nanomembrane topography modify the cell shape toward characteristics found in living tissue. We demonstrate the importance of substrate dimensionality for the migration mode of NSCs and thereby define rolled-up nanomembranes as the ultimate tool for single-cell migration studies.

KEYWORDS: Nanomembranes, rolled-up nanotechnology, 3D cell culture scaffold, spatial confinement, neural stem cells, cell migration
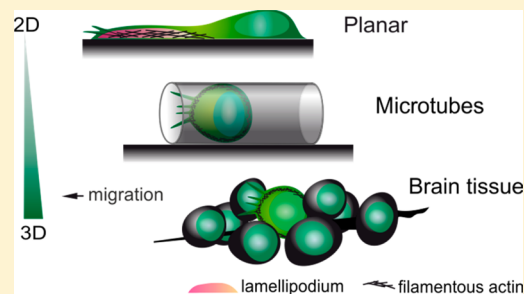
Regulated migration of cells is crucial for the correct development and tissue homeostasis of multicellular organisms. Although cell movement has been studied on two-dimensional (2D) substrates, the inferred findings can only to some extent help to understand the mechanisms that drive cell migration *in vivo*.[1] Importantly, the three-dimensional (3D) architecture of tissues cannot be reflected in the 2D nature of planar substrates,[2−5] where migrating cells possess an artificial apical−basal polarity with adhesions only formed at the basolateral side of the cells.[6] To address this issue, *in vitro* cell culture scaffolds have been designed to investigate cell migration strategies in a 3D context.[2] Hydrogels composed of either natural or synthetic fibrillar proteins have been employed frequently to study cell migration in a 3D environment.[7−10] However, hydrogel characteristics like porosity and compliance influence the cell migration response, and the deduction of a purely dimensionality-dependent scaffold effect remains challenging. To determine the mere impact of environment dimensionality on cell behavior, it is therefore desirable to exclude any additional influence caused by complex scaffold properties. More reductionistic cell culture scaffolds can help to reproduce distinct features of the extracellular environment and to separately infer their respective impact on cell migration. Micropatterned model systems like microchannels,[11−14] micropillars[15] or 3D free-form constructs[16,17] have for example been

fabricated to demonstrate that the topography of the scaffolds affects cell morphology and orientation as well as motility and migration mechanism. However, because of their inherent asymmetric (e.g., rectangular) design, these model systems fail to provide a homogeneous, completely surrounding cell environment. Scaffolds that completely encompass cells[18,19] are usually limited in their optical transparency and therefore the study of single-cell motility.

Another property that is tightly linked to scaffold dimensionality is the physical restriction of cell movement through the 3D topography. This confinement *in vivo* causes cells to employ different strategies like enzymatic matrix degradation or adapted cytoskeletal organization to navigate through tissues.[1,20,21] It was for instance shown that a protease-inhibitor treatment targeting the matrix degradation ability of tumor cells alone was not effective in stopping cancer spreading.[22−25] Similarly, cell confinement mediated by sandwiching cells between two nonadhesive surfaces led to a switch in migration phenotype in several cell lines instead of preventing cell movement.[26] In an attempt to classify morphologically distinct migration phenotypes, the terms
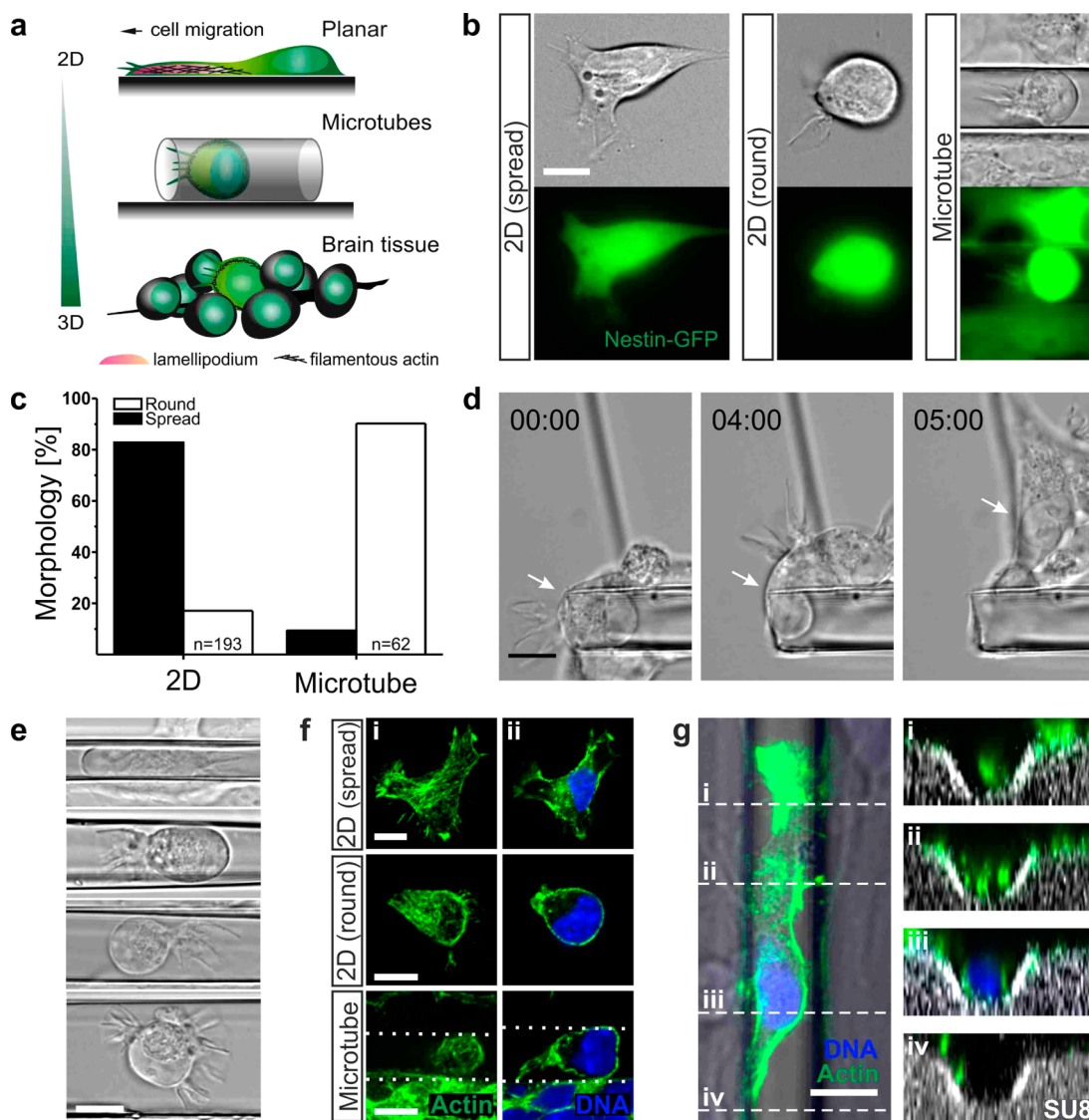
Figure 1. Dimensionality of the environment dictates NSCs morphology. (a) Schematic depicting the varying appearance of NSCs in different environments. (b) Differential interference contrast (DIC) and fluorescence top view images of a spread (left panel) and rounded (middle panel) NSC on a planar substrate compared to a round NSC inside a microtube (right panel). (c) Percentage of cells with spread or round morphology on planar (2D) substrates and inside microtubes. (d) DIC images of the morphology transition of an NSC leaving a microtube. The three different time points are indicated as h:min, white arrows highlight the cell (Supplementary Video S1). (e) DIC images of a single NSC inside a microtube with increasing diameter (top to bottom: 7/12/14/23 μm). (f) Fluorescence images of the actin cytoskeletal organization within a focal plane (i) next to the contact area of the cell and the substrate or (ii) at half of the cell height. The dotted white lines indicate the position of the microtube walls. (g) Left panel: overlay of the DIC and fluorescence top view images of an NSC growing within a 13 μm wide and 7 μm deep trench. The dashed white lines (i–iv) indicate the positions of the cut views (xz-plane) shown in the right panels. The SU8 fluorescence facilitates the visualization of the substrate in the cut views. All scale bars equal 10 μm.

mesenchymal and amoeboid migration modes have emerged. Mesenchymal migration is commonly found for spread cells on planar substrates and relies on a tight cell anchorage to the surface via focal adhesions. Amoeboid-like migration on the contrary is found for low-adhesive, rounded cells[27,28] and is mechanistically less well-defined, ranging from contractility-driven blebbing motility to purely actin polymerization-driven gliding.[29,30] Geometrically well-defined cell culture scaffolds can help to identify the cell type-dependent plasticity of migration strategies in response to physical confinement and to investigate the mechanistic differences in more detail. Overall, cells show a marked plasticity in 3D migration strategies, and a precise control of physical parameters of the cell environment

will be necessary for the investigation of tissue-relevant migration characteristics.

So far, cell migration has not yet been studied under a well-defined, more than one-dimensional (1D) isotropic confinement. To address this issue, we employed nanopatterning and strain-engineering of prestressed glass nanomembranes to confront cells with a 3D, tubular environment of defined dimensions. The optically transparent microtubes have already been shown to support the growth of human osteosarcoma U2OS cells[31] and to allow for the study of HeLa cell division in confined space.[32] Here we demonstrate that rolled-up nanomembranes are ideally suited as 3D scaffolds for neural stem cell (NSC) motility studies under determinable 2D confinement. Although only a tight regulation of NSC proliferation,
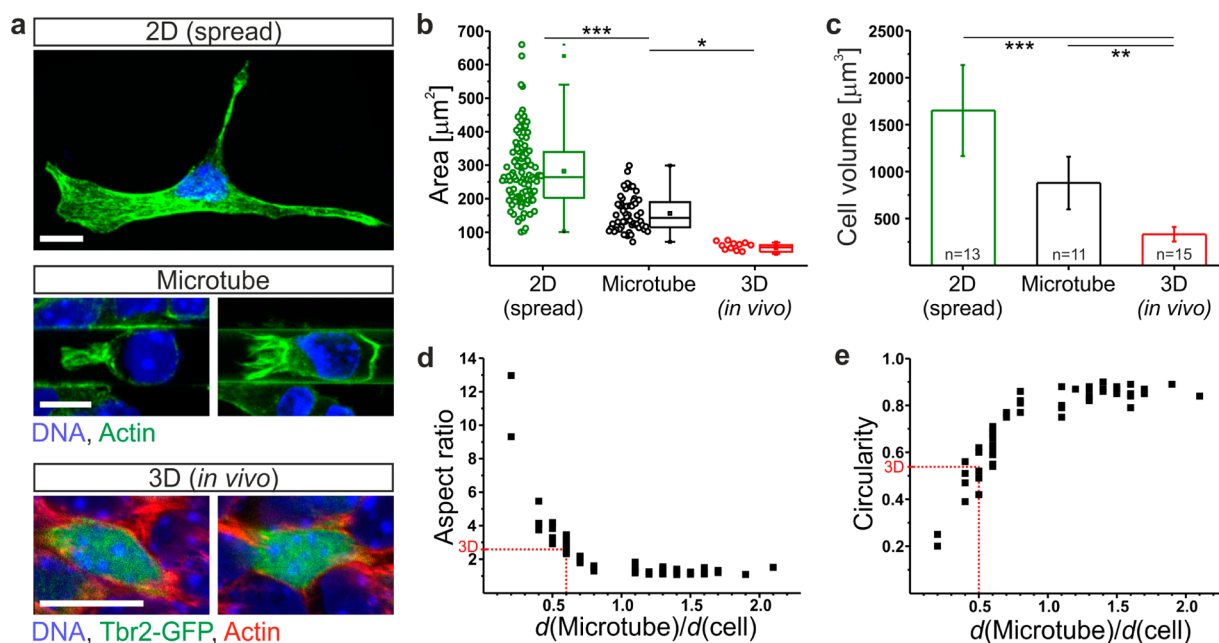
Figure 2. Comparison of *in vitro* cell shapes with *in vivo* morphology. (a) Slices of *z*-stacks for the 3D reconstruction of the immunofluorescently labeled cell bodies on a planar substrate, inside a microtube, and in brain tissue (for 3D reconstructions, please see Supplementary Video S3). The scale bars equal 10 μm. (b) Cell spread area of NSCs growing on planar (2D) substrates, inside microtubes, and in the developing brain *in vivo* (3D). Each data set is depicted as a scatter and a Tukey box plot (the box frames data between the 25th and 75th percentiles; the line shows the median; the square, the mean value, and the whiskers indicate the upper and lower fence of the data set). * $p < 0.05$; ** $p < 0.01$; *** $p < 0.001$ (Kruskal–Wallis test followed by Dunn's post test). (c) Cell volumes of NSCs growing on a planar substrate, inside microtubes, and in the 3D environment of the developing brain *in vivo* (cells are oriented in the *x-y* plane). Error bars show the SD for n = the number of cells indicated in the figures. (d, e) Dependence of the shape descriptors aspect ratio (long to short axis length of the projection area) and circularity (1 for a perfect circle) on the confinement (microtube to cell diameter ratio). In red color, parameters of the 3D *in vivo* situation are indicated.

migration, and differentiation leads to the correct structuring of the central nervous system, especially the brain,[33] the migration of NSCs that give rise to cortical neurons has not gained much attention yet. It is known that subclasses of neuronal progenitor cells localize to at least two proliferative layers in the brain,[34−37] but how the translocation of the progenitor cells takes place remains elusive.[38] Therefore, we study the spontaneous migration of murine NSCs within single-cell confining, 3D rolled-up nanomembranes with life-cell imaging. We observe that the scaffold dimensionality leads to a morphologically distinct mesenchymal to amoeboid migration mode transition for NSCs entering a microtube. *In vivo* studies confirm the convergence toward a native cell morphology for cells being confined by the microtube walls. Interestingly, we observe the absence of lamellipodia protrusions in the 3D environment, although the 3D locomotion strategy of NSCs is still dependent mainly on actin polymerization. Thereby, we provide experimental evidence that the planarity of traditional cell culture substrates is a factor that introduces artificial deviation from cell morphology and motility observed in live tissues. Strain engineering of nanomembranes offers the means to study single cell migration characteristics in a 3D context and to mimic the space-restricting aspect of the native cell environment.

In conventional 2D murine NSC culture protocols, cells are routinely cultured as a monolayer on fibronectin-coated polystyrene substrates.[39] The spread cell morphology observed on planar substrates differs strikingly from the appearance of cells in brain tissue, which we tried to mimic *in vitro* by confining NSCs within cylindrical microtubes (Figure 1a). The microtube structures were fabricated by angular deposition of

silicon monoxide/silicon dioxide nanomembranes onto a photolithographically structured polymer sacrificial layer and selective dissolution of the polymer.[40] Because of the chosen deposition parameters, the nanomembrane bilayer was prestressed and, upon release, self-assembled into an array of tubular structures (for details, please see Supporting Information). We demonstrate here that fibronectin-functionalized glass microtube substrates were suitable for the culture of NSCs and could sustain their undifferentiated character for more than 1 week (Supplementary Figure S1a, Supporting Information). On the planar regions of the microtube samples, we observed the reported predominant spread and fibroblastic as well as a less frequent small and round cell morphology[38] (Figure 1b). Surprisingly, the rounded morphology prevailed for NSCs that had entered one of the microtubes, where 90% of the cells were round compared to only 17% on the planar (2D) substrate (Figure 1b,c). Importantly, the round phenotype was not associated with cell death, as was proven with life-dead staining and the observation of cell divisions (Supplementary Figure S1b,c). The morphology transition occurred reversibly so that upon leaving the microtube environment, the round cells elongated and spread again (Figure 1d; Supplementary Video S1). Moreover, we observed that the microtube confinement modified the cell shape (Figure 1e). If the microtube diameter was larger than the spherical NSCs, cells were not restricted in the lateral and vertical directions by the tubular structure. When the microtube diameter was smaller, cells experienced a 2D confinement that was conveyed by the microtube walls, leading to an elongation of the round cell body.
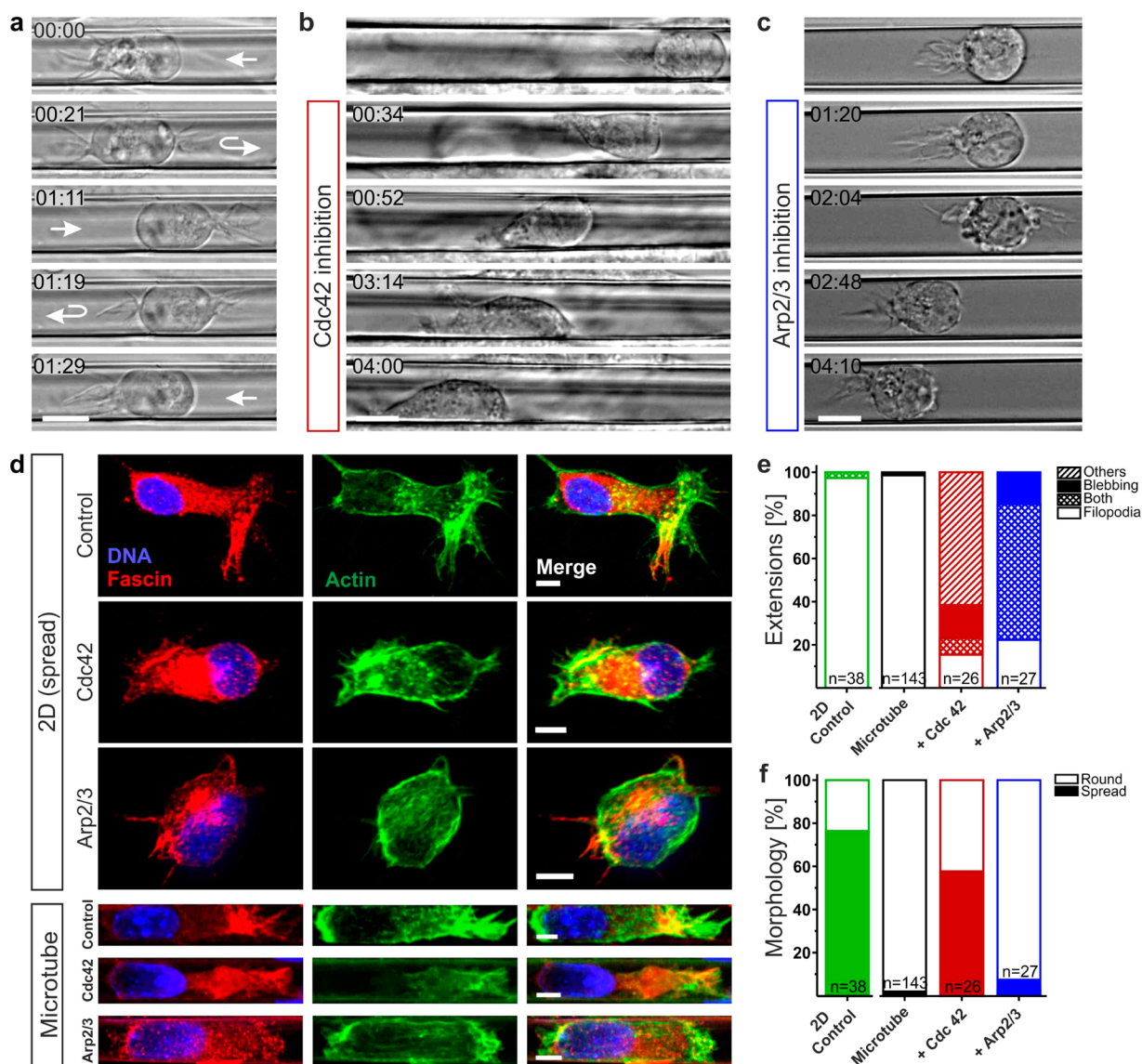
Figure 3. Cell morphology upon inhibition of filopodia (Cdc42 inhibitor) or lamellipodia (Arp2/3 complex inhibitor). For simplicity, only the abbreviated name of the inhibited protein is given. (a) DIC images at different time points (h:min) depicting an NSC that migrates within a microtube and changes its direction twice (Supplementary Video S4). (b, c) DIC image series (time points after drug treatment, h:min) of a Cdc42 inhibitor or Arp2/3 complex inhibitor treated NSC, respectively. The top image shows each cell before addition of the drug. Scale bars equal 10 μm, please see as well Supplementary Videos S5 and S6. (d) Comparison of the fluorescent staining for actin (cytoskeleton) and fascin (filopodia) in control and inhibitor treated cells either on a planar substrate or within a microtube. The scale bars equal 5 μm each. (e) Percentage of cells that show filopodia or blebbing, or no specific structures at the cell periphery ("Others"). (f) Percentage of cells with spread or round morphology for the indicated conditions. n = number of quantified cells.

Since the morphology of a cell is supported by its cytoskeleton, we investigated the respective distribution of actin filaments for the different morphology types either next to the contact region with the sample surface or at half of the cell height (Figure 1f). On the planar surface, it became obvious that thickened actin fibers were present in the contact region for both spread and rounded cells, whereas for completely spherical NSCs inside the microtubes, the confocal imaging did not resolve the actin organization into pronounced stress fibers. This indicates a tight anchoring of the cells to the planar substrate[1] that is not required inside the microtubes. To investigate whether the cell rounding and reduced anchorage to the substrate was caused by the curvature of the microtube walls rather than the increased dimensionality of the microtube topography, we fabricated trenches with comparable surface characteristics like roughness and functionalization to provide the curvature without the dimensionality aspect (Figure 1g). The trenches did not trigger the cell rounding that we had observed inside the microtubes. Instead, the cells elongated along the recess on the bottom of the structure (Supplementary Video S2). We therefore conclude that the dimensionality of the microtube topography triggers the rounded cell morphology. Although it is reckoned that the dimensionality of a scaffold is a crucial cell fate determinant, experimental evidence that directly addresses the influence of scaffold dimensionality on cell behavior is still scarce due to the inherent complexity of 3D systems. In extracellular matrix (ECM)-derived or ECM-mimicking hydrogels, for example, the polymer content and matrix cross-linking correlate directly with matrix stiffness, pore size, and therefore cell restriction and number of adhesion

sites,[3] which all have the potential to impact cell functioning. Additionally, the matrix composition of the scaffold material itself can introduce discrepancies, which was for instance shown for human bone marrow stromal cell morphology[41] or fibroblast adhesion and migration.[8] In a recent approach where single fibroblasts were cultured in 3D polydimethylsiloxane (PDMS) microwells[42] or on 2D microfabricated adhesive islands, Ochsner et al.[43] showed that the dimensionality and rigidity of the cell environment in dependence of each other affected actin organization and cell metabolism. In this context, strain-engineering and 3D assembly of nanomembranes offer a straightforward approach to create cell culture scaffolds that match 2D control substrates in material and surface functionalization so that adhesion site density, substrate stiffness, and composition are alike. The microtube samples differ from the planar substrates only in their topographical structuring so that the 3D assembled nanomembranes provides the means to microscopically observe the impact of scaffold dimensionality on cell response.

It is generally thought that 3D cell culture scaffolds allow for the deduction of more physiologically relevant mechanisms.[44] However, only a comparison to the situation in the tissue assesses the relevance for the real *in vivo* environment. We therefore compared the observed cell phenotypes with NSCs grown in their native brain environment (Figure 2).

The *in vitro* grown NSCs were fixed and stained for filamentous actin to visualize the cell body. For *in vivo* reference experiments, we prepared fixed brain sections of E14 mouse embryos expressing GFP-labeled Tbr2, a transcription factor found in proliferating and migrating intermediate progenitor cells in the neocortex.[45,46] Fluorescence imaging at different focal planes (*z*-stacks, Figure 2a) allowed for the 3D reconstruction of cell shapes (Supplementary Video S3) and the analysis of cell spread area (Figure 2b) as well as volume (Figure 2c). While the culturing of NSCs on the 2D substrate led to a multitude of cell spread areas, indicating various different cell shapes and an increase in cell volume not observed in the native environment, the microtube framework helped to counteract these peculiarities. Inside microtubes, cell volumes were significantly reduced toward values of densely packed cells in native brain tissue, and because of the prevalence of the round morphology, the distribution of cell shapes was narrower than on the planar surface. This demonstrates that the increase in topographical information is already sufficient to trigger a more *in vivo* relevant NSC morphology, although the rigidity of the glass microtubes is much larger than the elasticity of brain tissue. To investigate this resemblance more closely, we analyzed measures of cell morphology with more emphasis on cell roundness (Figure 2d,e). The aspect ratio (Figure 2d) relates the long axis of the cell projection area to its short axis, and the circularity (Figure 2e) describes in how far this area resembles a perfect circle (circularity = 1). Since we observed the modification of the round cell shape by the microtube width (compare Figure 1e), we took into account the dependence on cell confinement, expressed as ratio of microtube to cell diameter. Unconfined NSCs (microtube to cell diameter ratio >1) were highly spherical with circularities and aspect ratios close to 1. With decreasing microtube diameter, the NSCs were forced into a more elongated and flattened shape so that the circularity values decreased, whereas the aspect ratio increased. When the microtube diameter was reduced to about half the size of unconfined spherical NSCs (d (cell) = 13.6 ± 0.7 μm, n = 30), the shape descriptors of the

confined cells approached the respective values of NSCs in the brain (circularity = 0.54 ± 0.07, aspect ratio = 2.6 ± 0.6, n = 11). Together with the small *in vivo* spread areas, this finding suggests that NSCs experience a certain confinement in the 3D environment of the developing brain where the space available for the growth of cells is limited. While the dimensionality of rolled-up nanomembranes prevents the artificial cell spreading found on planar substrates, the microtube confinement fine-tunes the cell morphology toward *in vivo*-like characteristics. This is supported by recent literature[47] that reports on a dense packing of cells in the neuroepithelium and that names 2D mechanical stress as one of the factors driving NSCs out of the layer of birth into their destined regions. Therefore, the rolled-up nanomembranes not only provide a cell-surrounding environment, but also can be designed to mimic space restrictions of the cell's native tissue.

During the observation of NSC behavior inside microtubes, it became evident that the round cell bodies always possessed filamentous structures protruding from the cell front and pointing in the direction of movement (Figure 3a; Supplementary Video S4). In contrary to the basal localization of cell extensions in spread NSPCs either on the planar substrate (Supplementary Video S3) or within the trenches (compare Figure 1g), these filamentous structures evolved from the center of the cell front and not close to the microtube bottom (Movie S3), hinting at the absence of apical−basal cell polarity within the microtubes.

For spread cells migrating across planar substrates, it is known that the cell front assumes different shapes but in most cases consists of a sheet of branched actin filaments named lamellipolium and bundled actin filaments at the leading edge termed filopodia. To identify the finger-like cell protrusions observed in the microtubes as filopodia and to clarify the presence of a lamellipodium, we studied the cell behavior under the influence of small molecule inhibitors that are known to impede the respective protrusions on 2D (Figure 3b,c; Supplementary Videos S5 and S6). We employed an inhibitor against Cdc42, a small GTPase that induces the formation of filopodia at the cell leading edge.[48,49] A second inhibitor was targeted against the Arp2/3 complex, which is an actin-binding protein that nucleates the branching of actin filaments in the lamellipodium.[50,51] Additionally, we used immunofluorescent staining of filamentous actin and the filament-bundling protein fascin, which is found in filopodia,[52] to visualize and identify cell protrusions (Figure 3d). For control cells on the planar substrate, the fluorescent staining revealed the presence of both a dendritic actin network in a spread lamellipodium as well as fascin-bundled actin filaments in filopodia at the cell front. For NSCs inside microtubes, however, the sheet-like lamellipodia structure could not be detected. Instead, the colocalization of filamentous actin and fascin identified the finger-like structures at the cell front as filopodia. Consistently, a Cdc42 inhibitor treatment caused the disappearance of the finger-like protrusions, while the reduction of the Arp2/3 complex activity did not prevent protrusion formation (Figure 3e). Strikingly, the filopodia inhibition additionally led to a reversal of cell rounding (Figure 3b), which was found for more than half of the treated cells (Figure 3f). The Arp2/3-activity reduced cells still maintained the rounded morphology with filopodia protrusions, occasionally disrupted by cell blebbing (Figure 3c). The appearance of blebs after Arp2/3 complex inhibition supports recent findings that this protein is involved in the maintenance of cell cortex integrity[53,54] and the control of
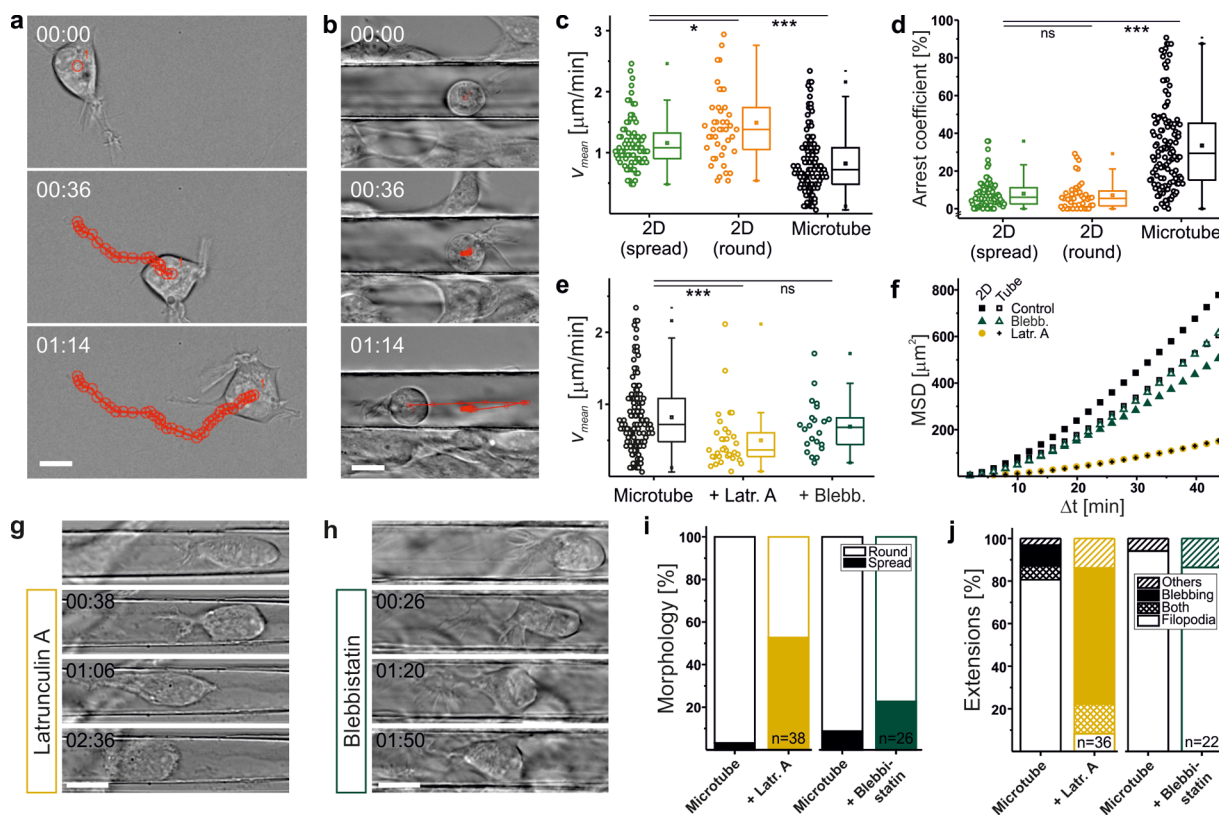
Figure 4. 2D versus 3D single cell migration characteristics of NSCs. (a, b) DIC images overlaid with the tracks of an NSC (a) on a planar substrate and (b) within a microtube at three different time points (h:min). Every red circle corresponds to the cell position tracked in 2 min time intervals. Please see as well Supplementary Videos S7 and S8. (c) Mean velocitiy v_{mean} and (d) arrest coefficient of cells that migrate on a planar (2D) substrate or within a microtube. For the planar substrate, the data are further discriminated according to the cell shape. The arrest coefficient is the proportion of time that the cells migrate slower than the critical velocity of 0.27 μm/min; ns, not significant; ∗ $p < 0.05$; ∗∗∗ $p < 0.001$ (Kruskal−Wallis test followed by Dunn's post test). (e) Mean cell velocity inside a microtube after inhibition of actin polymerization (latrunculin A) or myosin contractility (blebbistatin). (f) Mean squared displacement (*MSD*) analysis averaged for 15−51 cell tracks. The influence of latrunctulin A and blebbistatin drugs on cell migration efficiency on a planar surface (filled markers) or inside microtubes is compared. (g, h) DIC image series (time points after drug treatment, h:min) of an actin polymerization or myosin II contractility inhibitor treated NSC inside a microtube. The top image shows each cell before addition of the drug. Please see as well Supplementary Videos S10 and S11. (i) Percentage of spread or round cells inside a microtube before and after the indicated inhibitor treatment. (j) Proportion of cells that show filopodia or bleb protrusions, or no specific structures at the cell periphery ("Others") upon actin polymerization or myosin contractility inhibition, respectively. All scale bars equal 10 μm.

cortical tension,[20] thus favoring bleb initiation upon Arp2/3 complex activity reduction.[55] We here monitored bleb formation on the entire surface of the cell, which contradicts the possibility of blebbing being an alternative movement strategy, which would require a polarized bleb emergence. Inside microtubes filopodia protrusions that are thought to fulfill sensory, exploratory and probing functions[56,57] prevail over the formation of a sheet-like lamellipodium that is associated with surface anchorage and persistent migration on planar substrates.[56] The exploratory cell activity is necessary for the maintenance of the round phenotype that is only observed as long as the cells are able to form the sensing organelles. Therefore, it is crucial to offer a 3D environment to cells to infer migration mechanisms that are not dominated by the artificial adaption to planar substrates. Here, the parallel processing of microtube arrays in an on-chip format and the spontaneous migration of NSCs into the rolled-up structures allowed us to simultaneously analyze the formed cell protrusions of several cells in parallel. Inhibitor treatment, live-cell imaging, and fluorescent immunostaining helped to characterize the cell protrusions in more detail and could be read out due to the compatibility of the glass nanomembranes with high-resolution optical microscopy.

Since the microtube scaffold had such a distinct effect on cell morphology, we speculated that the NSC interaction with the microtube topography could modify their motility as well. The optical transparency of the glass microtubes and the ability to design their dimensions in the fabrication process make them an ideal structure to study spontaneous migration of single cells in different degrees of confinement. Spontaneous migration is the cell movement that is initiated randomly without the presence of external guidance cues ("matrix-induced")[58] and thereby allows the observation of the mere topography-triggered cell behavior not overridden by external guidance cues, for example, biochemical or physical stiffness gradients. We took time-lapse images of NSCs that were moving on planar substrates or within the microtubes and tracked their positions in 2 min time intervals for up to 4 h (Figure 4a,b; Supplementary Videos S7 and S8). The acquired tracks on the planar substrate showed constant step distances, indicating continuous cell motion with a steady velocity, while inside the microtubes, the NSC movement became more irregular. To assess these differences quantitatively, we calculated the mean velocity (Figure 4c) as well as the arrest coefficient (Figure 4d) for each cell track. The arrest coefficient is the percentage of

time that the cells were slower than a critical velocity[59] of 0.27 μm/min.

The analysis revealed that the spherical cells on the planar surface moved fastest and inside the microtube slowest. The arrest coefficients for NSCs on 2D substrates did not differ significantly and were much smaller than the arrest coefficients inside the microtubes. For the planar substrate, these findings are in line with the characteristics of the mesenchymal migration mode. The necessary surface anchorage via a broad lamellipodium counteracts cell mobility. Cells with a rounded cell body have a reduced contact area with the substrate (compare Figure 1f) and can thereby achieve higher migration velocities at comparable arrest coefficients. In line with this reasoning, the cells inside the microtubes with completely spherical cell bodies should be able to migrate at least at similar rates. However, the average cell velocities were smaller, and the arrest coefficients of the cells significantly increased, hinting at a different cell migration strategy. Additionally, we observed only a minor correlation of cell velocity and arrest coefficient with cell confinement. Only inside very small microtubes (diameter ratio < 0.5) the NSCs were appreciably slowed down and displayed bleb formation at both cell ends (Supplementary Video S9), confirming theoretical modeling that predicts a threshold confinement for a stable cell membrane to cortex attachment.[60] This implies a direct impact of scaffold dimensionality, rather than cell confinement, on the observed migration characteristics of NSCs. This is in line with recent evidence derived mainly from 1D migration models mimicking fibrillar 3D matrices, indicating that cell migration depends on the dimensionality of the ECM.[3,61] These models demonstrated for fibroblasts that the 3D phenotype resembled mechanistically more the 1D uniaxial than a 2D migration.[7,62,63] Although imparting valuable insight into migration mechanisms, these patterned lines or 1D fibers still induced an artificial apical–basal cell polarity. Taken together, the findings indicate that although spontaneous migration is a prominent cell characteristic on planar substrates, it might not represent cell motility in tissues already, due to the lack of 3D topographic information, that we could provide the cells with inside the rolled-up glass nanomembranes.

The observed differences in actin cytoskeleton organization, migration strategies, and especially the remarkable differences in cell morphology are characteristic of a mesenchymal to amoeboid migration mode transition.[24,64] The amoeboid migration mode is usually associated with an increased contribution of cell contractility and blebbing motility but can also rely on mainly actin polymerization.[20,30] To assess the relative importance of the two mechanisms for the 3D migration mode of NSCs, we investigated the impact of latrunculin A, which inhibits the polymerization of actin filaments, and blebbistatin, which counteracts cell contractility, on migration characteristics of the cells. Interfering with the actin polymerization led to a significant reduction of mean cell migration velocities (Figure 4e) and a decreased migration efficiency (Figure 4f). More than half of the cells spread again inside the microtubes (Figure 4g,i), and filopodia formation was greatly reduced (Figure 4j, Supplementary Video S10). A reduction of cell contractility through blebbistatin treatment, however, did not change the migration characteristics (Figure 4e, f) or cell morphology and protrusion formation (Figure 4i,j) remarkably inside the microtubes. We only observed a prolonged attachment of the cell membrane to the microtube walls characteristic for a reduced cell contractility (Figure 4h,

Supplementary Video S11), which overall did not prevent cell motility. This indicates that NSC amoeboid migration mainly depends on an actin polymerization mechanism and that weaker substrate contacts are established, which upon reduction of cell contractility can still be detached. This is in contrast to the 2D mesenchymal migration mode, where a stronger cell anchoring to the substrate requires higher cell contractility for contact detachment, and the blebbistatin treatment counteracts locomotion (Figure 4f). This compares to the finding that NSC migration in the *in vivo* brain environment is not continuous and comprises distinct phases of pausing, forward, and retrograde movement,[34] similar as in the microtube environment. Radial migration velocities *in vivo* were reported to range from 0.10 $\pm$ 0.01 μm/min to 0.33 $\pm$ 0.10 μm/min[34] and are therefore slower than the measured velocities on 2D substrates or within the microtube samples, most likely because neither *in vitro* substrate did confine cell movement in all three dimensions. Additionally, brain tissue is much softer than the glass substrates employed in this study so that the rigidity or substrate elasticity is likely to further impact NSC migration characteristics.[43,65] In follow-up studies, it remains to be clarified which substrate parameters affect cell behavior to what extent and ultimately how their interplay modifies cell migration *in vivo*. Our studies demonstrate that the dimensionality of the cell culture substrate is crucial for the employed migration mode of the NSCs and that physical space restrictions of the cell environment must be taken into account. The fabrication of glass microtubes by strain-engineering of selectively released nanomembranes offers the means to design a geometrically well-defined cell environment for the study of cell migration under 2D isotropic, native tissue-mimicking space restrictions. The potential to incorporate additional functionalities in the rolled-up fabrication process, like structured electrodes for impedance sprectroscopy,[66] and the microfluidic integration of glass microtubes that as well can act as optofluidic sensors,[67] provides a versatile system with the ultimate aim to study 3D cell responses in a lab-in-a-tube[68] approach. This will facilitate the study of fundamental aspects of 3D cell migration characteristics that are crucial for embryonic development as well as immune surveillance, and are defective in fatal processes like cancer metastasis.

In summary, we demonstrate that strain-engineering and self-assembly of glass nanomembranes offer a straightforward approach to fabricate a neural stem cell culture-compatible, 3D environment with well-defined geometry. By applying this reductionist 3D cell culture scaffold and thereby imposing a 2D confinement on single cells, we could approach the *in vivo* cell morphology. Changing just the dimensionality of the cell environment triggered a profound change in NSC morphology and motility characteristics. The NSCs possessed a high plasticity in cell shape that became apparent with the morphologically distinct mesenchymal to amoeboid migration mode transition, but a low plasticity in actin polymerization-dependent protrusion formation. Our findings advance the comparison of traditional 2D cell culture, 3D biomaterial scaffolds, and physiological cell environment with the focus on discerning spatial aspects of the *in vivo* tissue that influence cell behavior. We demonstrate that strain-engineering and self-assembly of nanomembranes enables the study of space-restricted, 3D cell migration characteristics with the future potential to further characterize the single-cell behavior in a lab-in-a-tube approach. Our results underline the need for careful identification, validation, and finally integration of essential

tissue properties to design *in vivo*-mimicking biomaterial scaffolds.

■ ASSOCIATED CONTENT

Ⓢ Supporting Information

A detailed description of experimental methods regarding scaffold fabrication, cell culture and drug treatment, immuno-cyto- and immunohistochemistry, as well as microscopic readout. List of microscopes employed for (live-cell) image acquisition and explanation of data analysis procedures. Images of a live/dead fluorescent NSC staining. Videos displaying NSC migration behavior under various conditions (e.g., inhibitor treatments). The Supporting Information is available free of charge on the ACS Publications website at DOI: 10.1021/acs.nanolett.5b02099.

■ AUTHOR INFORMATION

Corresponding Author

*E-mail: b.koch@ifw-dresden.de.

Present Address

S.S., Institut de Bioenginyeria de Catalunya (IBEC), 08028 Barcelona, Spain; Institució Catalana de Recerca i Estudis Avancats (ICREA), 08010 Barcelona, Spain.

Author Contributions

A.K.M., S.S., and O.G.S conceived the project, B.K. and A.K.M. designed experiments. B.K., L.H., and A.K.M. performed research, and A.S. contributed new reagents/analytic tools. B.K. and A.K.M. analyzed data with help from L.H. S.S. and O.G.S. supervised the project. The manuscript was written through contributions of all authors. All authors have given approval to the final version of the manuscript.

Notes

The authors declare no competing financial interest.

■ ACKNOWLEDGMENTS

■ REFERENCES

(1) Friedl, P.; Brocker, E. B. *Cell. Mol. Life Sci.* **2000**, *57*, 41−64.
(2) Baker, B. M.; Chen, C. S. *J. Cell Sci.* **2012**, *125*, 3015.
(3) Doyle, A. D.; Petrie, R. J.; Kutys, M. L.; Yamada, K. M. *Curr. Opin. Cell Biol.* **2013**, *25*, 642−649.
(4) Webb, D. J.; Horwitz, A. F. *Nat. Cell Biol.* **2003**, *5*, 690−692.
(5) Even-Ram, S.; Yamada, K. M. *Curr. Opin. Cell Biol.* **2005**, *17*, 524−532.
(6) Beningo, K. A.; Dembo, M.; Wang, Y.-l. *Proc. Natl. Acad. Sci. U. S. A.* **2004**, *101*, 18024−18029.
(7) Doyle, A. D.; Wang, F. W.; Matsumoto, K.; Yamada, K. M. *J. Cell Biol.* **2009**, *184*, 481−490.
(8) Hakkinen, K.; Harunaga, J.; Doyle, A.; Yamada, K. *Tissue Eng., Part A* **2011**, *17*, 713−724.
(9) Miron-Mendoza, M.; Seemann, J.; Grinnell, F. *Biomaterials* **2010**, *31*, 6425−6435.
(10) Grinnell, F.; Ho, C.-H.; Tamariz, E.; Lee, D. J.; Skuta, G. *Mol. Biol. Cell* **2003**, *14*, 384−395.
(11) Pathak, A.; Kumar, S. *Proc. Natl. Acad. Sci. U. S. A.* **2012**, *109*, 10334−10339.
(12) Kaiser, J.-P.; Reinmann, A.; Bruinink, A. *Biomaterials* **2006**, *27*, 5230−5241.
(13) Balzer, E. M.; Tong, Z.; Paul, C. D.; Hung, W. C.; Stroka, K. M.; Boggs, A. E.; Martin, S. S.; Konstantopoulos, K. *FASEB J.* **2012**, *26*, 4045−56.
(14) Hawkins, R. J.; Piel, M.; Faure-Andre, G.; Lennon-Dumenil, A. M.; Joanny, J. F.; Prost, J.; Voituriez, R. *Phys. Rev. Lett.* **2009**, *102*, 058103.
(15) Ghibaudo, M.; Trichet, L.; Le Digabel, J.; Richert, A.; Hersen, P.; Ladoux, B. *Biophys. J.* **2009**, *97*, 357−368.
(16) Olsen, M. H.; Hjortø, G. M.; Hansen, M.; Met, O.; Svane, I. M.; Larsen, N. B. *Lab Chip* **2013**, *13*, 4800−4809.
(17) Schneider, J.; Bachmann, T.; Franco, D.; Richner, P.; Galliker, P.; Tiwari, M. K.; Ferrari, A.; Poulikakos, D. *Macromol. Biosci.* **2013**, *13*, 973−983.
(18) Knight, T.; Basu, J.; Rivera, E. A.; Spencer, T.; Jain, D.; Payne, R. *Cell Adh Migr* **2013**, *7*, 267−274.
(19) Lin, J.-y.; Lin, W.-j.; Hong, W.-h.; Hung, W.-c.; Nowotarski, S. H.; Gouveia, S. M.; Cristo, I.; Lin, K.-h. *Soft Matter* **2011**, *7*, 10010−10016.
(20) Bergert, M.; Chandradoss, S. D.; Desai, R. A.; Paluch, E. *Proc. Natl. Acad. Sci. U. S. A.* **2012**, *109*, 14434−14439.
(21) Wolf, K.; te Lindert, M.; Krause, M.; Alexander, S.; te Riet, J.; Willis, A. L.; Hoffman, R. M.; Figdor, C. G.; Weiss, S. J.; Friedl, P. *J. Cell Biol.* **2013**, *201*, 1069−1084.
(22) Sahai, E.; Marshall, C. J. *Nat. Cell Biol.* **2003**, *5*, 711−719.
(23) Yamazaki, D.; Kurisu, S.; Takenawa, T. *Oncogene* **2009**, *28*, 1570−1583.
(24) Wolf, K.; Mazo, I.; Leung, H.; Engelke, K.; von Andrian, U. H.; Deryugina, E. I.; Strongin, A. Y.; Bröcker, E.-B.; Friedl, P. *J. Cell Biol.* **2003**, *160*, 267−277.
(25) Friedl, P.; Wolf, K. *Nat. Rev. Cancer* **2003**, *3*, 362−374.
(26) Liu, Y.-J.; Le Berre, M.; Lautenschlaeger, F.; Maiuri, P.; Callan-Jones, A.; Heuzé, M.; Takaki, T.; Voituriez, R.; Piel, M. *Cell* **2015**, *160*, 659−672.
(27) Yoshida, K.; Soldati, T. *J. Cell Sci.* **2006**, *119*, 3833−3844.
(28) Smith, L. A.; Aranda-Espinoza, H.; Haun, J. B.; Dembo, M.; Hammer, D. A. *Biophys. J.* **2007**, *92*, L58−L60.
(29) Lämmermann, T.; Sixt, M. *Curr. Opin. Cell Biol.* **2009**, *21*, 636−644.
(30) Friedl, P.; Wolf, K. *J. Cell Biol.* **2010**, *188*, 11−19.
(31) Koch, B.; Sanchez, S.; Schmidt, C. K.; Swiersy, A.; Jackson, S. P.; Schmidt, O. G. *Adv. Healthcare Mater.* **2014**, *3*, 1753−8.
(32) Xi, W.; Schmidt, C. K.; Sanchez, S.; Gracias, D. H.; Carazo-Salas, R. E.; Jackson, S. P.; Schmidt, O. G. *Nano Lett.* **2014**, *14*, 4197−204.
(33) Wade, A.; McKinney, A.; Phillips, J. J. *Biochim. Biophys. Acta, Gen. Subj.* **2014**, *1840*, 2520−5.
(34) Noctor, S. C.; Martinez-Cerdeno, V.; Ivic, L.; Kriegstein, A. R. *Nat. Neurosci.* **2004**, *7*, 136−144.
(35) Haubensak, W.; Attardo, A.; Denk, W.; Huttner, W. B. *Proc. Natl. Acad. Sci. U. S. A.* **2004**, *101*, 3196−201.
(36) Miyata, T.; Kawaguchi, A.; Saito, K.; Kawano, M.; Muto, T.; Ogawa, M. *Development* **2004**, *131*, 3133−3145.
(37) Liu, X.; Hashimoto-Torii, K.; Torii, M.; Haydar, T. F.; Rakic, P. *Proc. Natl. Acad. Sci. U. S. A.* **2008**, *105*, 11802−11807.
(38) Lyu, J.; Hu, Y. n.; Xu, X.; Zhang, H. *J. Cell. Biochem.* **2013**, *114*, 1744−1759.
(39) Meyer, A. K.; Jarosch, A.; Schurig, K.; Nuesslein, I.; Kissenkotter, S.; Storch, A. *Brain Res.* **2012**, *1474*, 8−18.
(40) Harazim, S. M.; Xi, W.; Schmidt, C. K.; Sanchez, S.; Schmidt, O. G. *J. Mater. Chem.* **2012**, *22*, 2878−2884.
(41) Farooque, T. M.; Camp, C. H., Jr; Tison, C. K.; Kumar, G.; Parekh, S. H.; Simon, C. G., Jr *Biomaterials* **2014**, *35*, 2558−2567.
(42) Ochsner, M.; Dusseiller, M. R.; Grandin, H. M.; Luna-Morris, S.; Textor, M.; Vogel, V.; Smith, M. L. *Lab Chip* **2007**, *7*, 1074−1077.
(43) Ochsner, M.; Textor, M.; Vogel, V.; Smith, M. L. *PLoS One* **2010**, *5*, e9445.

(44) Pampaloni, F.; Reynaud, E. G.; Stelzer, E. H. K. *Nat. Rev. Mol. Cell Biol.* **2007**, *8*, 839−845.

(45) Englund, C.; Fink, A.; Lau, C.; Pham, D.; Daza, R. A. M.; Bulfone, A.; Kowalczyk, T.; Hevner, R. F. *J. Neurosci.* **2005**, *25*, 247−251.

(46) Gotz, M.; Huttner, W. B. *Nat. Rev. Mol. Cell Biol.* **2005**, *6*, 777−788.

(47) Okamoto, M.; Namba, T.; Shinoda, T.; Kondo, T.; Watanabe, T.; Inoue, Y.; Takeuchi, K.; Enomoto, Y.; Ota, K.; Oda, K.; Wada, Y.; Sagou, K.; Saito, K.; Sakakibara, A.; Kawaguchi, A.; Nakajima, K.; Adachi, T.; Fujimori, T.; Ueda, M.; Hayashi, S.; Kaibuchi, K.; Miyata, T. *Nat. Neurosci.* **2013**, *16*, 1556−1566.

(48) Nobes, C. D.; Hall, A. *J. Cell Biol.* **1999**, *144*, 1235−1244.

(49) Surviladze, Z.; Waller, A.; Strouse, J. J.; Bologa, C.; Ursu, O.; Salas, V.; Parkinson, J. F.; Phillips, G. K.; Romero, E.; Wandinger-Ness, A.; Sklar, L. A.; Schroeder, C.; Simpson, D.; Noth, J.; Wang, J.; Golden, J.; Aube, J. A Potent and Selective Inhibitor of Cdc42 GTPase. In *Probe Reports from the NIH Molecular Libraries Program*; National Center for Biotechnology Information: Bethesda, MD, 2010.

(50) Nolen, B. J.; Tomasevic, N.; Russell, A.; Pierce, D. W.; Jia, Z.; McCormick, C. D.; Hartman, J.; Sakowicz, R.; Pollard, T. D. *Nature* **2009**, *460*, 1031−1034.

(51) Suraneni, P.; Rubinstein, B.; Unruh, J. R.; Durnin, M.; Hanein, D.; Li, R. *J. Cell Biol.* **2012**, *197*, 239−251.

(52) Vignjevic, D.; Kojima, S.-i.; Aratyn, Y.; Danciu, O.; Svitkina, T.; Borisy, G. G. *J. Cell Biol.* **2006**, *174*, 863−875.

(53) Machesky, L. M.; Insall, R. H. *Curr. Biol.* **1998**, *8*, 1347−1356.

(54) Salbreux, G.; Charras, G.; Paluch, E. *Trends Cell Biol.* **2012**, *22*, 536−545.

(55) Charras, G.; Paluch, E. *Nat. Rev. Mol. Cell Biol.* **2008**, *9*, 730−736.

(56) Mejillano, M. R.; Kojima, S.-i.; Applewhite, D. A.; Gertler, F. B.; Svitkina, T. M.; Borisy, G. G. *Cell* **2004**, *118*, 363−373.

(57) Mattila, P. K.; Lappalainen, P. *Nat. Rev. Mol. Cell Biol.* **2008**, *9*, 446−454.

(58) Takagi, H.; Sato, M. J.; Yanagida, T.; Ueda, M. *PLoS One* **2008**, *3*, e2648.

(59) Boissonnas, A.; Fetler, L.; Zeelenberg, I. S.; Hugues, S.; Amigorena, S. *J. Exp. Med.* **2007**, *204*, 345−56.

(60) Lim, F. Y.; Koon, Y. L.; Chiam, K.-H. *Comput. Methods Biomech. Biomed. Eng.* **2013**, *16*, 1085−1095.

(61) Friedl, P.; Sahai, E.; Weiss, S.; Yamada, K. M. *Nat. Rev. Mol. Cell Biol.* **2012**, *13*, 743−747.

(62) Chang, Stephanie S.; Guo, W.-h.; Kim, Y.; Wang, Y.-l. *Biophys. J.* **2013**, *104*, 313−321.

(63) Doyle, A. D.; Kutys, M. L.; Conti, M. A.; Matsumoto, K.; Adelstein, R. S.; Yamada, K. M. *J. Cell Sci.* **2012**, *125*, 2244−2256.

(64) Huang, B.; Lu, M.; Jolly, M. K.; Tsarfaty, I.; Onuchic, J.; Ben-Jacob, E. *Sci. Rep.* **2014**, *4*, 6449.

(65) Solon, J.; Levental, I.; Sengupta, K.; Georges, P. C.; Janmey, P. A. *Biophys. J.* **2007**, *93*, 4453−4461.

(66) Martinez-Cisneros, C. S.; Sanchez, S.; Xi, W.; Schmidt, O. G. *Nano Lett.* **2014**, *14*, 2219−2224.

(67) Harazim, S. M.; Bolanos Quinones, V. A.; Kiravittaya, S.; Sanchez, S.; Schmidt, O. G. *Lab Chip* **2012**, *12*, 2649−2655.

(68) Smith, E. J.; Xi, W.; Makarov, D.; Monch, I.; Harazim, S.; Bolanos Quinones, V. A.; Schmidt, C. K.; Mei, Y.; Sanchez, S.; Schmidt, O. G. *Lab Chip* **2012**, *12*, 1917−1931.